JOC The Journal of Organic Chemistry

Article

pubs.acs.org/joc

Absolute Configuration of Native Oligomeric Proanthocyanidins with Dentin Biomodification Potency

Joo-Won Nam,[†,⊥] Rasika S. Phansalkar,[†] David C. Lankin,[†] James B. McAlpine,[†,‡] Ariene A. Leme-Kraus,[§] Cristina M. P. Vidal,[§] Li-She Gan,[∥] Ana Bedran-Russo,[§] Shao-Nong Chen,[†,‡] and Guido F. Pauli*[,†,‡]

[†]Department of Medicinal Chemistry & Pharmacognosy and [‡]Institute for Tuberculosis Research, College of Pharmacy, University of Illinois at Chicago, Chicago, Illinois 60612, United States

[§]Department of Restorative Dentistry, College of Dentistry, University of Illinois at Chicago, Chicago, Illinois 60612, United States

[∥]College of Pharmaceutical Sciences, Zhejiang University, Hangzhou 310058, People's Republic of China

[⊥]College of Pharmacy, Yeungnam University, Gyeongsan, Gyeongbuk 712-749, Korea

Supporting Information

ABSTRACT: The structurally complex oligomeric proanthocyanidins (OPACs) are promising biomimetic agents, capable of strengthening the macromolecular backbone of teeth via intermolecular and intermicrofibrillar cross-linking. This study establishes analytical methods capable of determining the absolute configuration of the catechin-type monomeric units of underivatized OPACs. This preserves the capacity of their biological evaluation, aimed at understanding the inevitably stereospecific interactions between the OPACs and dentin collagen. Guided by dental bioassays (modulus of elasticity, long-term stability), two new trimeric and tetrameric A-type OPACs were discovered as dentin biomodifiers from pine (*Pinus massoniana*) bark: epicatechin-(2β→*O*→7,4β→8)-epicatechin-(2β→*O*→7,4β→8)-catechin (**5**) and epicatechin-(2β→*O*→7,4β→8)-epicatechin-(2β→*O*→7,4β→6)-epicatechin-(2β→*O*→7,4β→8)-catechin (**6**), respectively. Combining 1D/2D NMR, HRESIMS, ECD, ^{1}H iterative full spin analysis (HiFSA), and gauge-invariant atomic orbital (GIAO) δ calculations, we demonstrate how ^{13}C NMR chemical shifts (diastereomeric building blocks (A-type dimers)) empower the determination of the absolute configuration of monomeric units in the higher oligomers **5** and **6**. Collectively, NMR with ECD reference data elevates the level of structural information achievable for these structurally demanding molecules when degradation analysis is to be avoided. Considering their numerous and deceptively subtle, but 3D impactful, structural variations, this advances the probing of OPAC chemical spaces for species that bind selectively to collagenous and potentially other biologically important biomacromolecules.

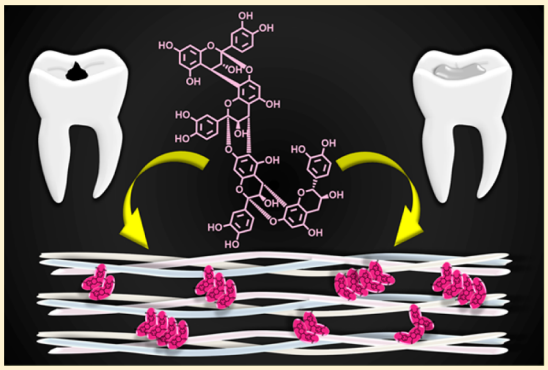

INTRODUCTION

The Chemistry−Dentistry Interface. Dental caries is the most widespread chronic disease worldwide that affects the vast majority of people during their entire lifetime.[1] For more than 120 years, amalgam restorations have been widely used to replace lost dental tissue caused by caries, with the advantages of low cost, ease of treatment, and extended durability (10−15+ years).[2,3] For cosmetic and safety (mercury exposure) reasons, amalgam has been replaced gradually by resin-based composites.[2] However, resin-based restorations are not ideal, as their lifespan is limited to 5−8 years due to secondary caries, biodegradation, and poor fracture resistance.[3,4] The unavoidable loss of the enamel in dental restoration explains why new strategies have to consider the crucial role of dentin, the bulk calcified extracellular tissue of the tooth, composed largely of type I collagen. Replacement of failed resin restorations gives rise to the additional loss of dentin structure and extra cost. Hence, a biomimetic approach capable of enhancing dentin's biomechanical properties by nonenzymatic collagen cross-linking at various hierarchical levels can be key to stabilizing the dentin−resin interface and result in increased longevity of the dental restoration.[5,6]

Plant Polyphenols as Potent and Safe Tissue Biomodifiers. Our long-term goal is to develop new biomaterials from natural sources that enhance the dentin collagen structure via chemical and/or physical molecular interactions. The present study focuses on chemical insights that are central to this interdisciplinary task, applied to the study of pine (*Pinus massoniana*) bark polyphenols as highly potent and biorenewable biomodifiers of dentin. This report is based on the outcomes of dentin bioassay-guided fractionation (BGF) of what otherwise is an agricultural waste product: the bark of pine (*Pinus massoniana* LAMB., Pinaceae). Isolation of

Received: September 2, 2016
Published: January 18, 2017

DOI: 10.1021/acs.joc.6b02161
J. Org. Chem. 2017, 82, 1316−1329

Scheme 1. Structures of the A-Type OPACs 1−6 from Pine Bark Characterized During This Study

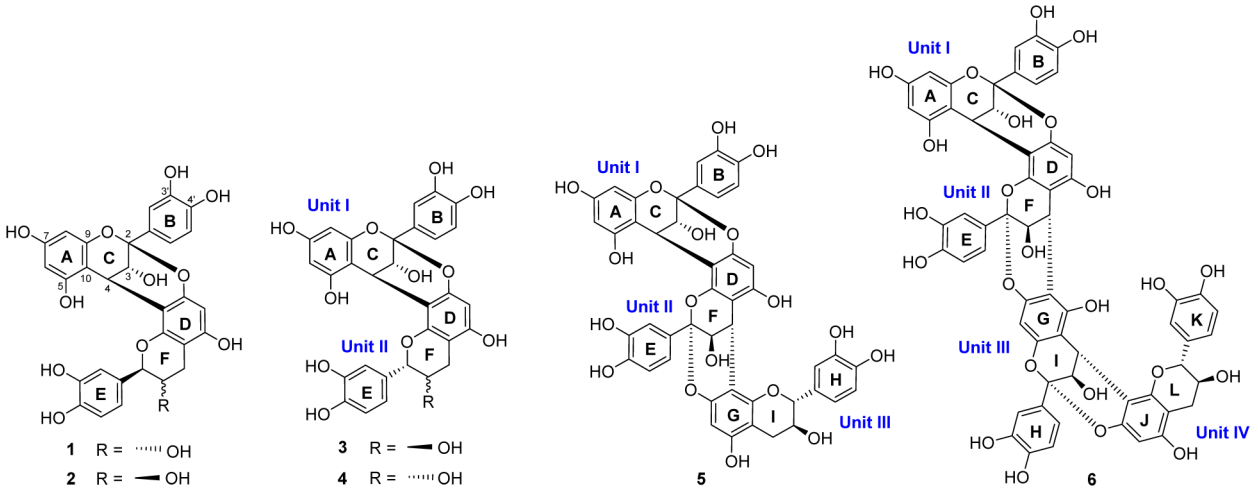

Table 1. Theoretical Structural Possibilities of Pine OPACs[a]

monomer type	interflavonoid connection type	structural possibility (P) of OPACs[b] DP = 2	DP = 3	DP = 4	DP = 5	DP = 6
catechin (C), *ent*-catechin (*ent* C), epicatechin (EC), *ent*-epicatechin (*ent* EC)	4α→8,4β→8	112	3,136	87,808	2,458,624	68,841,472
	4α→6,4β→6					
	2→O→7,4→8[c]					
	2→O→7,4→6[c]					
	2→O→5,4→6[c]					

[a]The calculations reflect the theoretical permutations on the basis of the constituting monomeric units, linkage types and sites (interflavonoid linkage), and the degree of polymerization (DP) known to occur in *P. massoniana*. These figures will increase further as structural motifs are discovered. OPACs from other plants are known to include further possibilities that act as multipliers. [b]Structural possibilities (P) of OPACs were calculated by the equation $P = m(mc)^{n-1}$, with m = number of general types of monomer units and c = number of possible connection types and positions. DP = degree of polymerization. [c]Each monomer unit has three possible doubly linked connections, which due to the relative configurations of C-2/C-4 were fixed as one of each 2α/4α and 2β/4β.

the dentin-enhancing oligomeric proanthocyanidins (OPACs) in their free-phenolic form is amenable to subsequent evaluation of their biomodification potency, structure elucidation of new bioactive trimers and tetramers, and assignment of their absolute configuration by NMR via chiral characterization of reference dimers and new ^{13}C-based diastereomeric evidence (Scheme 1).

The development of long-lasting biomaterials to be directly embedded in the human oral cavity also requires the consideration of safety parameters. In general, in comparison with synthetic materials, natural products can frequently fulfill this role by showing relatively low cytotoxicity. OPACs are plant polyphenols with recently demonstrated activity in enhancing the modulus of elasticity of dentin.[7,8] The interaction between collagen and OPAC molecules leads to the formation of biocompatible cross-linked structures. This stabilizes the dentin−resin interface and thus enhances the restoration. In addition, OPAC mixtures exhibit bioadhesive properties to dentin and contribute to increased longevity of adhesive dental restorations.[9] Recently, we identified medium-length OPACs (n = 3−4) from distinct plant sources, including grape seeds, cinnamon bark, and pine bark, as potent plant-derived collagen cross-linkers.[10−12] In particular, the trimeric PAC *ent*-epicatechin-(4β→8)-epicatechin-(2β→O→7,4β→8)-catechin isolated from the bark of *Pinus massoniana* has shown promise and presents the most potent dentin biomodification activity observed of a single chemical entity so far.[11]

Structural and Analytical Complexity of OPACs. Also known as condensed tannins, OPACs consist of repeating flavan-3-ol monomeric building blocks. Condensation into (higher) oligomers and polymers occurs via interflavanyl linkages mainly through one (C→C; B-type) and/or two (C→C and C→O→C; A-type) single-bond connections.[13,14] Although not immediately evident from the relatively simple building pattern, OPACs exhibit an exceptionally large number of structural variations. Even when the number is limited to medium-chain analogues up to DP = 6, the combination of various monomers, linkage positions/types, and degrees of polymerization (DP) forms a giant chemical space as the molecules extend. Accordingly, the isolation and characterization of a single OPAC molecule, especially in free phenolic form and for DP ≥ 3, continues to be a preparative and analytical chemistry challenge. Moreover, all constituting monomers possess two stereogenic centers, resulting in a myriad of OPAC diastereomers and enantiomers, and one extra stereogenic element is added with each atropisomeric interflavonoid linkage.

Hence, the determination of the complete *absolute* configuration of an OPAC is a gargantuan task. At the same time, this level of chemical knowledge is of importance, considering the profound chirality of the target biomacromolecule (dentin/collagen), as well as the observed specificities

DOI: 10.1021/acs.joc.6b02161
J. Org. Chem. 2017, 82, 1316−1329

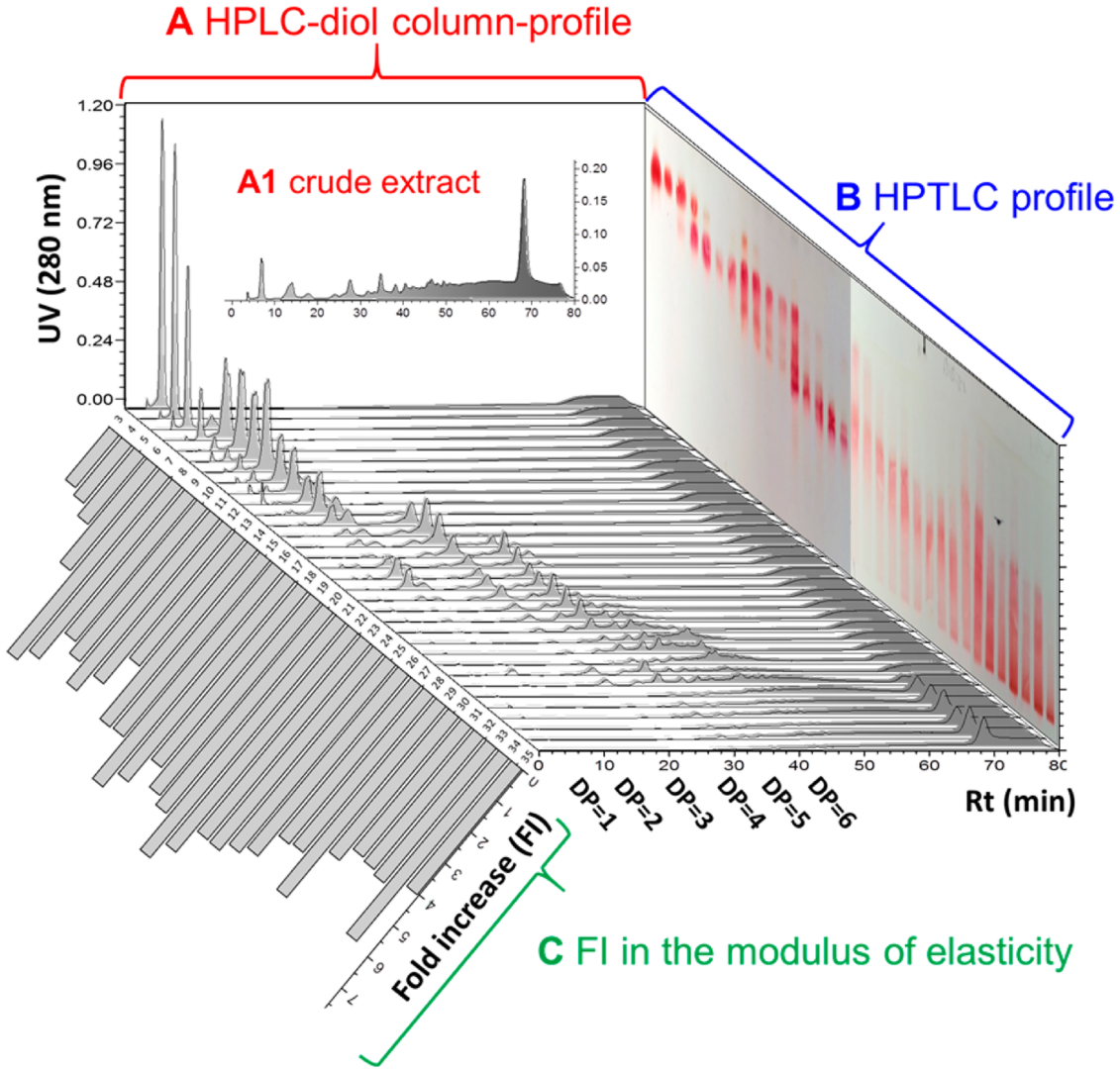

Figure 1. 3D representation of the preparative VLC fractionation and dentin mechanical properties of *P. massoniana* extract. The fractions were profiled by HPLC using a diol column (A and floor; A-1 is the crude extract) and by HPTLC (B). The biochromatogram in (C) represents fold increases in the apparent modulus of elasticity of dentin. DPs of the fractions were further analyzed by MS analysis. The broad HPLC peaks (A) and unsharp HPTLC bands (B) reflect the huge structural space to be expected from the complex biosynthetic permutations, as outlined in Table 1.

and variation of potencies of certain plant proanthocyanidin preparations. For the present case of pine bark, >68000000 hypothetical OPAC hexamers exist, and even trimers and tetramers challenge chromatographic and spectroscopic analysis with >3000 and >80000 potential distinct structures, respectively (Table 1).

Another important consideration affecting our understanding of the chemistry of these potent bioactives relates to the means of structural documentation: 2D structural drawings of OPACs look superficially similar; Scheme 1 may already serve as an example. However, the 3D shape of each molecule is clearly distinct, and so can be its biological potential. The spatial specificity of each OPAC undoubtedly determines its cross-linking potency (or lack thereof) in the chiral environment of the target peptide, collagen, and other dentin-associated molecules. However, in most cases the stereochemistry of OPACs has not been determined rigorously but rather assumed on the basis of biosynthesis considerations, which in turn for OPACs are based on relatively limited experimental evidence relative to other natural product classes.

One approach to define the complete absolute configuration of OPACs involves their depolymerization or degradation and subsequent identification of the monomeric units.[15,16] However, degradative methods suffer from the inherent flaw of invariably involving the breaking of bonds that are critical to the overall properties of the intact molecules. In addition, losses due to degradation are an impediment to their interdisciplinary study, as they make the dental (or any other biological) evaluation of bioactive compounds impossible. In the present research, a new approach was developed for determining the relative and absolute configuration of isolated A-type OPACs by a nondestructive method using ^{13}C NMR chemical shifts, in combination with electronic circular dichroism (ECD) experiments. The results were further confirmed by quantum-mechanical (QM) calculations.

RESULTS AND DISCUSSION

Fractionation of Pine Extract. In order to fractionate the pine bark OPACs mainly according to their degree of polymerization (DP), the extract was first subjected to vacuum column chromatography (VLC) using silica gel as the

DOI: 10.1021/acs.joc.6b02161
J. Org. Chem. 2017, 82, 1316−1329

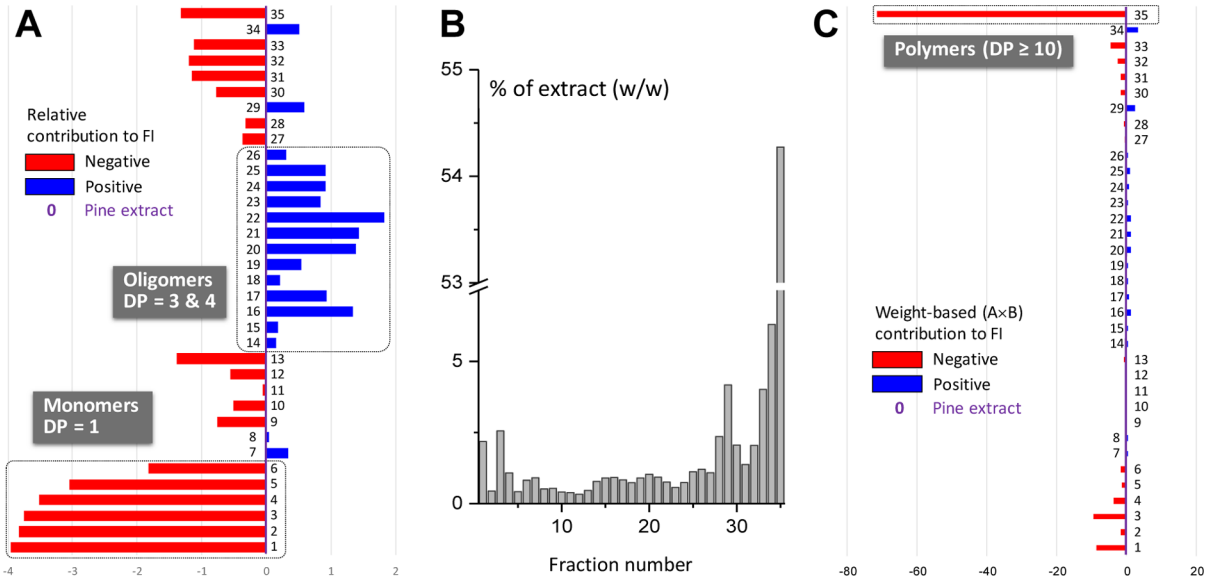

Figure 2. Summary of dentin bioassay results used to prioritize the primary fractions of *P. massoniana* extract. (A) Fold increase (FI) in the apparent modulus of elasticity of the fractions normalized to the FI of crude pine extract. The FI was calculated as the FI ratio after vs before treatment (final vs base value). The weight distribution of the fractions (B; % w/w) and the weight-normalized FI contributions (C) show that both the monomeric and polymeric PACs are abundant but ineffective, whereas certain OPAC fractions (14–26, 29) contain the main dentin bioactive principles of pine bark.

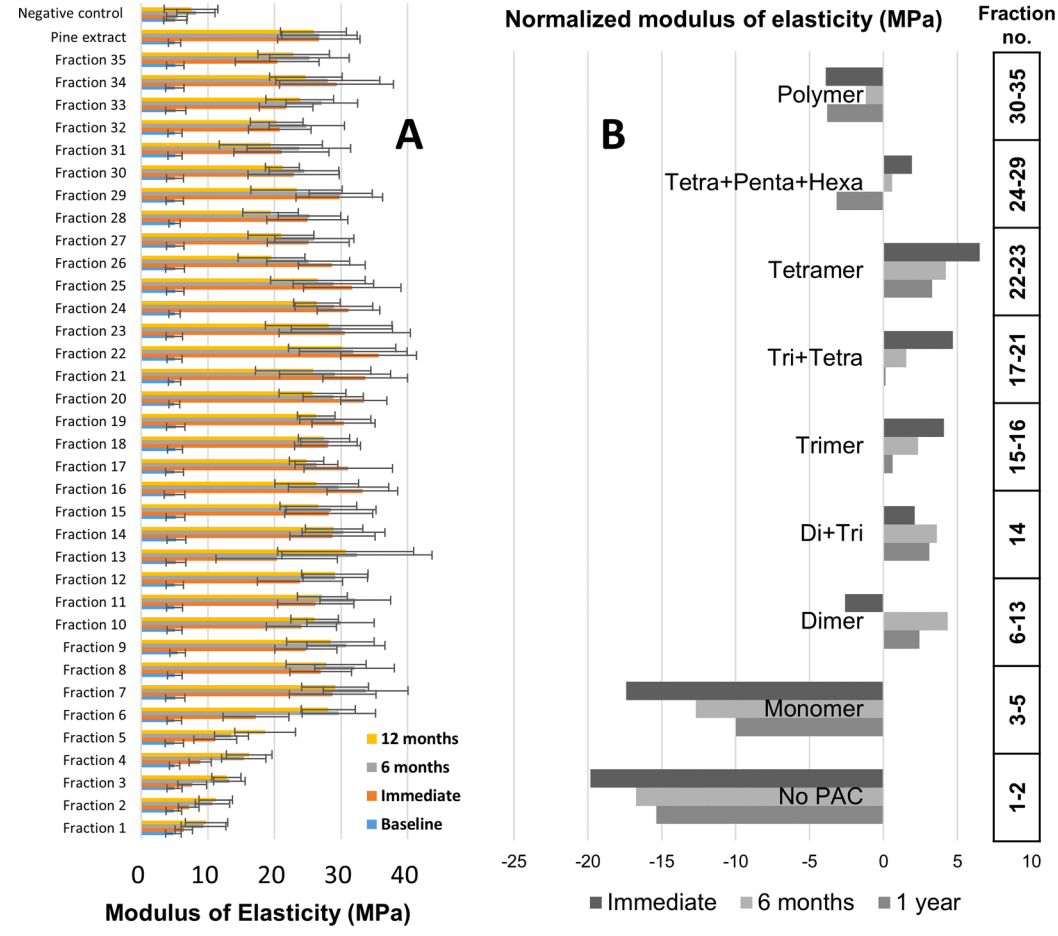

Figure 3. Long-term stability of dentin biomodification by the primary VLC fractions: (A) modulus of elasticity (MPa) of 35 fractions assessed at 0 (immediate), 6, and 12 months post treatment; (B) modulus of elasticity grouped by DP (see Figure 1) and assessed at 0, 6, and 12 months post treatment. The apparent modulus of elasticity (MPa) of each group was normalized to the activity of the pine bark extract.

DOI: 10.1021/acs.joc.6b02161
J. Org. Chem. 2017, 82, 1316–1329

Table 2. ^{1}H and ^{13}C NMR (900/225 MHz, resp.) Spectroscopic Data of Compounds 3 and 4[a,b]

			3		4	
unit	ring	no.	δ_C, mult	δ_H, mult (J, Hz)	δ_C, mult	δ_H, mult (J, Hz)
I	C	2	100.42, C		100.45, C	
		3	67.68, CH	4.1242, d (3.4)	67.78, CH	4.1570, d (3.4)
		4	29.26, CH	4.2381, d (3.4)	29.27, CH	4.4012, d (3.4)
	A	5	156.69, C		156.66, C	
		6	98.13, CH	5.9241, d (2.3)	97.94, CH	5.8819, d (2.3)
		7	158.19, C		158.15, C	
		8	96.57, CH	6.0526, d (2.3)	96.53, CH	6.0562, d (2.3)
		9	154.10, C		154.16, C	
		10	104.03, C		104.07, C	
	B	1′	132.23, C		132.34, C	
		2′	115.61, CH	7.1389, dd (2.2, 0.2)	115.61, CH	7.1433, dd (2.2, 0.2)
		3′	145.67, C		145.69, C	
		4′	*146.82, C		146.81, C	
		5′	115.72, CH	6.8132, dd (8.2, 0.2)	115.71, CH	6.8169, dd (8.2, 0.2)
		6′	119.84, CH	7.0226, dd (8.2, 2.2)	119.84, CH	7.0291, dd (8.2, 2.2)
II	F	2	83.91, CH	4.7368, dd (8.1, −0.8)	80.86, CH	5.0245, dd (1.4, −0.8)
		3	68.41, CH	4.0570, ddd (8.8, 8.1, 5.1)	67.16, CH	4.2400, ddd (4.3, 2.1, 1.4)
		4	28.88, CH_2	2.9584, dd (−16.3, 5.1)	29.51, CH_2	2.9094, dd (−16.9, 4.3)
				2.5570, dd (−16.3, 8.8)		2.8521, dd (−16.9, 2.6)
	D	5	156.18, C		156.75, C	
		6	96.51, CH	6.0772, s	96.44, CH	6.0828, s
		7	152.24, C		152.10, C	
		8	106.54, C		106.94, C	
		9	150.85, C		151.31, C	
		10	102.80, C		101.89, C	
	E	1′	130.93, C		131.43, C	
		2′	115.42, CH	6.9598, dd (2.0, 0.3)	115.21, CH	7.1258, dd (2.1, 0.4)
		3′	146.44, C		146.25, C	
		4′	*146.78, C		146.25, C	
		5′	116.32, CH	6.8378, dd (8.1, 0.3)	116.16, CH	6.8365, dd (8.2, 0.4)
		6′	120.32, CH	6.8565, ddd (8.1, 2.0, −0.8)	119.40, CH	6.9450, ddd (8.2, 2.1, −0.8)

[a] ^{1}H and ^{13}C NMR data were acquired in methanol-d_4 at 298 K and at 900 and 225 MHz, respectively. [b] The δ_H and J values including their signs were generated via ^{1}H iterative full spin analysis (HiFSA; for pms profiles, see the Supporting Information).[11] Asterisks indicate that the assignments are interchangeable.

stationary phase. An aqueous solvent system (dichloromethane−methanol with 1% water) was utilized because OPACs are relatively polar molecules even at DP = 2. The VLC fractions were characterized by IT-TOF MS, HPLC (diol-column), and HPTLC, allowing their classification according to the DP (Figure 1). The weight distribution of the fractions evident from Figure 2B indicated that polymeric PACs accounted for >50% (w/w) of the crude extract.

Dentin Mechanical Properties Create Biochromatograms. Evaluation of all VLC fractions (Figure 2) in the dentin mechanical properties bioassay assessed the fold increase (FI) of the apparent modulus of elasticity of the dentin matrix. Biochromatograms were constructed which were normalized to the enhancement of dentin mechanical properties of the crude extract (Figure 2A) and the weight contribution of each fraction (Figure 2C). This revealed clearly that the fractions enriched in trimeric and tetrameric PACs were the predominant contributors to the bioactivity and, thus, contained the main active principles. The blue and red bars in Figure 2 represent the positive and negative contributions of each fraction to the bioactivity of the extract, respectively. While representing a large proportion of the whole extract, monomeric and polymeric PACs exhibited lower activities than the extract. Therefore, the further bioassay-guided fractionation strategy concentrated on the isolation of bioactives from fractions containing medium-DP OPACs.

Important evidence for the biological relevance of certain medium-DP OPAC fractions came from studies that assessed the long-term stability of the observed dentin biomodification. Measuring the apparent modulus of elasticity of the dentin beams at three different time points, immediately after biomodification/treatment as well as after 6 and 12 months, generated the long-term biochromatogram in Figure 3A. For the purpose of investigating the effect of the DP on the mechanical properties, the results of the apparent modulus of elasticity assays of the 35 VLC fractions were clustered into nine groups according to their DPs (Figures 1 and 3B). The long-term stability data further support the prioritization of the fractions containing trimeric and tetrameric PACs for the isolation of bioactive marker compounds. The remarkable long-term stability indicates that the PAC−dentin interactions are highly stable, holding promising application for dentin repair.

Isolation of the Pine OPACs 3−6. A series of gravity and flash NP silica gel columns, Sephadex LH-20 columns, and reverse-phase semipreparative HPLC separations was used to purify individual OPACs from the active primary VLC fractions 14−26. This led to the isolation of two new A-type OPACs, epicatechin-(2β→O→7,4β→8)-epicatechin-(2β→O→7,4β→

DOI: 10.1021/acs.joc.6b02161
J. Org. Chem. 2017, 82, 1316−1329

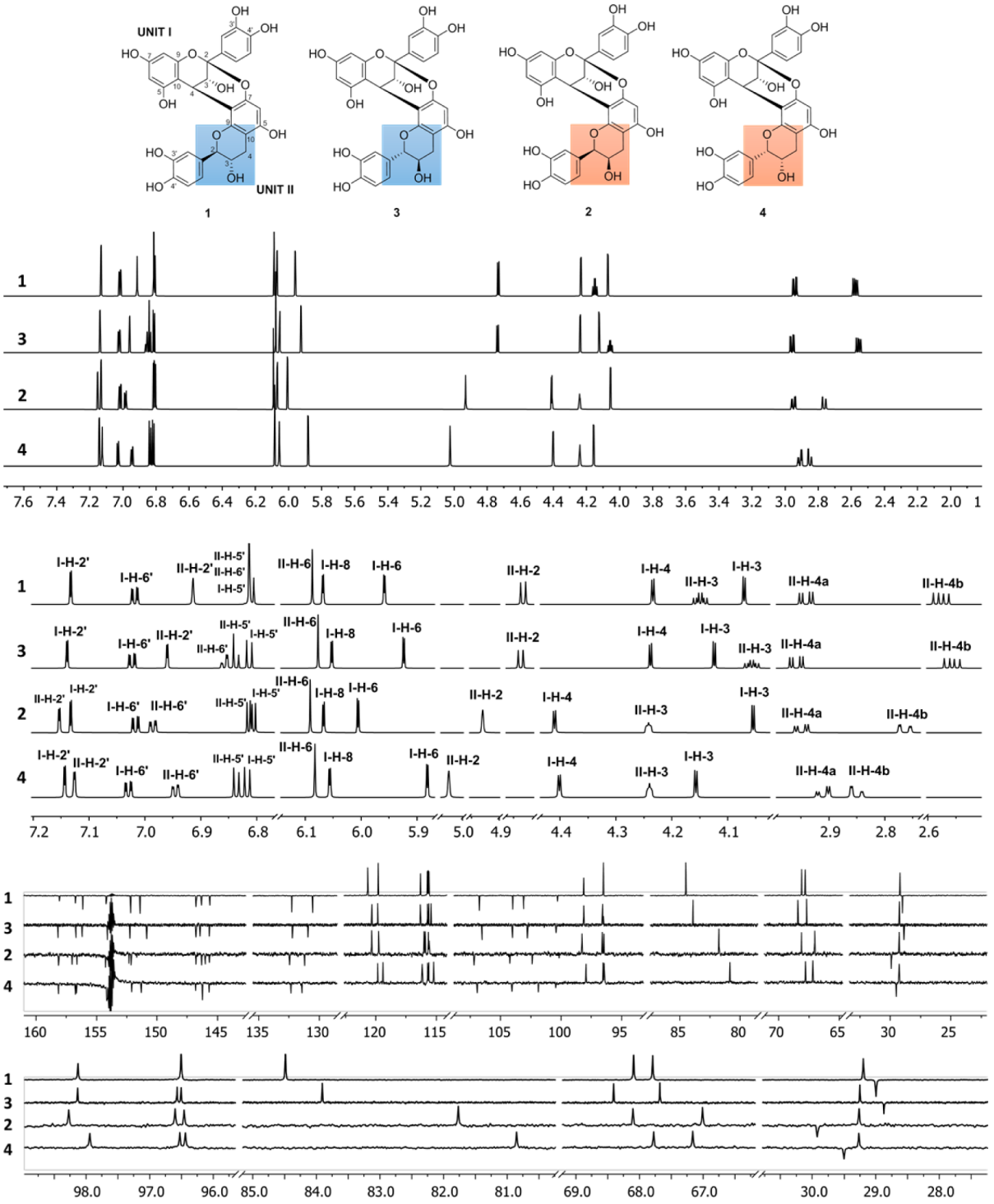

Figure 4. Full and expanded plots of the ^{1}H NMR (HiFSA fingerprints; 900 MHz) and ^{13}C DEPTQ (225 MHz) NMR spectra of the dimeric OPACs **1**–**4**. The structures at the top show the distinctive stereochemical features of **1**–**4** marked in ring F. The out-of-phase signals at ~154 ppm are solvent image artifacts that are common in high dynamic range DEPTQ spectra.

8)-catechin (**5**) and epicatechin-(2*β*→*O*→7,4*β*→8)-epicatechin-(2*β*→O→7,4*β*→6)-epicatechin-(2*β*→*O*→7,4*β*→8)-catechin (**6**), together with two known dimeric PACs, epicatechin-(2*β*→*O*→7,4*β*→8)-*ent*-catechin (proanthocyanidin A4, **3**) and epicatechin-(2*β*→*O*→7,4*β*→8)-*ent*-epicatechin (**4**).[17−19] The structures of the isolates were elucidated by a combination of HR-ESI-MS, ECD, 1D and 2D NMR, and ^{1}H iterative full spin analysis (HiFSA). In addition, the purities (%, w/w) of **3**–**6** were determined by qHNMR to be 95.3, 90.5, 89.6, and 80.4%, respectively, using the 100% method (Figures S1−S4 in the Supporting Information).[20]

Full ^{1}H and ^{13}C NMR Assignments of the Dimers 3 and 4 as References. Although representing known compounds, in order to serve as references for absolute configuration, the structures of **3** and **4** had to be elucidated ab initio, including their full chirality. Their molecular formulas were determined by HR-ESI-MS to be $C_{30}H_{24}O_{12}$, supporting **3** and **4** to be doubly linked dimeric PACs. The ^{1}H (900 MHz)

DOI: 10.1021/acs.joc.6b02161
J. Org. Chem. 2017, 82, 1316−1329

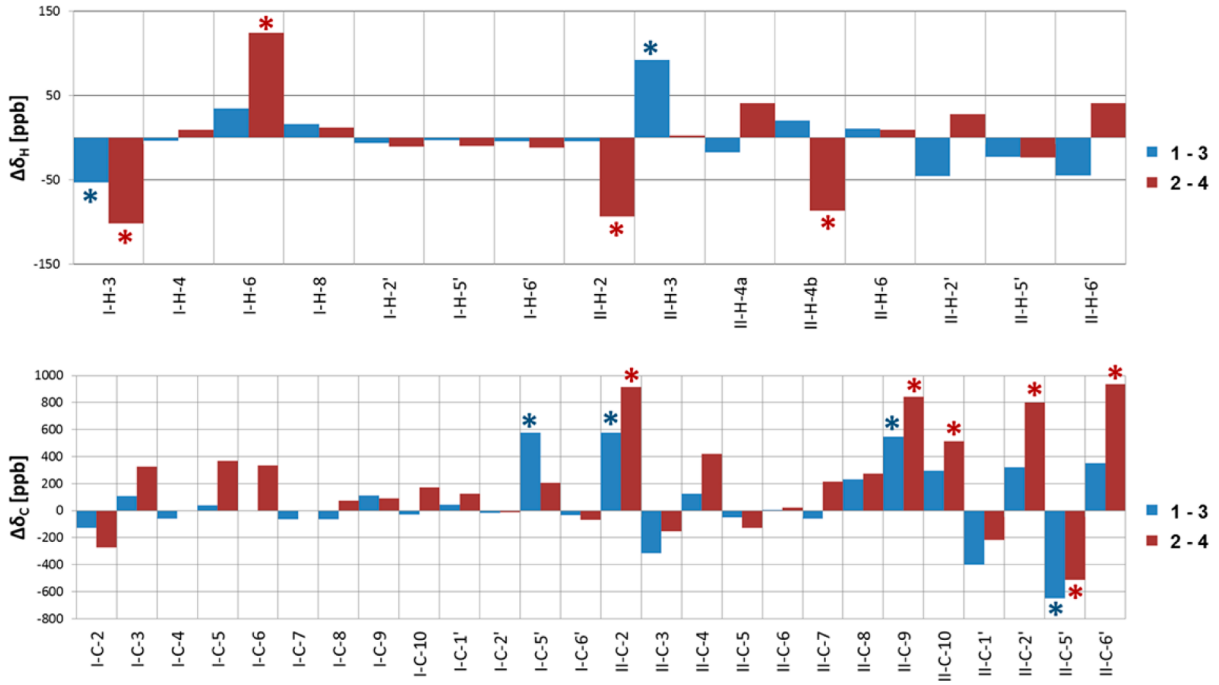

Figure 5. Graphical representation of the ^{1}H and ^{13}C chemical shift differences ($\Delta\delta$) between the diastereomeric pairs **1**/**3** (blue) and **2**/**4** (red) expressed in ppb. ^{1}H and ^{13}C NMR data were acquired in CD_3OD at 298 K and at 900 and 225 MHz, respectively. The chemical shift differences of C-3′ and C-4′ were excluded due to their interchangeable assignments. Asterisks denote diagnostic $\Delta\delta$ values that allow differentiation between the diastereomeric pairs **1**/**3** and **2**/**4**.

and ^{13}C DEPTQ-135 (225 MHz) NMR spectra of **3** and **4** were similar to those of proanthocyanidins A1 (**1**) and A2 (**2**), respectively, except for some minor but characteristic differences in the chemical shifts (Table 2).[11,17] The presence of 2→*O*→7/4→*8* doubly linked interflavanyl bonds rather than 2→*O*→7/4→*6* bonds was established by the HMBC cross-peaks from H-4 (C ring) to C-7, C-8, and C-9 (D ring). This was further supported by NOE correlations between H-4 (C ring) and H-2 (F ring), and H-4 (C ring) and H-2′ (E ring) in both **3** and **4**. The 4*β* configuration (C ring) in **3** and **4** was gleaned from strong positive ECD Cotton effects at 223 nm.[21,22] From the observation of a large vicinal coupling ($^{3}J_{2H,3H}$ = 8.14 Hz), the relative configurations of H-2/H-3 in the F ring of **3** was established as trans, resembling closely the configuration in **1** ($^{3}J_{2H,3H}$ = 7.88 Hz).[11] In comparison to **1** and **3**, the ^{1}H NMR spectra of **4** showed a small vicinal coupling between the F ring protons of $^{3}J_{2H,3H}$ < 2 Hz, suggesting that the lower flavan-3-ol unit in **4** is 2,3-cis configured, as in **2**.[11]

The collective NMR evidence suggested that **3** and **4** were C-2/C-3 (F ring) diastereoisomers of **1** and **2**, thus containing *ent*-catechin (2*S*,3*R*) and *ent*-epicatechin (2*S*,3*S*), respectively, as the lower units. Subsequently, complete assignment of the ^{1}H and ^{13}C NMR resonances was performed by a combination of 2D NMR (COSY, HSQC, HMBC, and ROESY) experiments (Figures S5−S16 in the Supporting Information). All evidence was most compatible with the structures epicatechin-(2*β*→O→7,4*β*→8)-*ent*-catechin (proanthocyanidin A4) for **3** and epicatechin-(2*β*→O→7,4*β*→8)-*ent*-epicatechin for **4**, known compounds that have not been isolated from *P. massoniana* previously.[17−19]

^{1}H NMR HiFSA Fingerprints of Diastereoisomeric OPAC Dimers. As shown recently, fully assigned ^{1}H NMR spectra can provide important pieces of evidence about the structures, stereochemistry, and chemical exchange properties of OPACs.[11] As the DP increases, starting already at DP = 2, the NMR spectra of OPACs progress toward being nearly identical. Accordingly, the determination of highly detailed ^{1}H NMR profiles becomes essential for their identification and distinction. One notable feature involves the ortho benzylic couplings of **3** ($^{4}J_{E\text{-}H\text{-}6',F\text{–}H\text{-}2}$ = −0.78 Hz) and **4** ($^{4}J_{E\text{-}H\text{-}6',F\text{–}H\text{-}2}$ = −0.79 Hz): established by HiFSA, these ^{4}J relationships between the aliphatic benzyl and their adjacent (ortho) aromatic protons are associated with negative coupling constants. Being a diagnostic feature of relative configuration, these small couplings are sufficiently large to be visualized as splittings by the use of Lorentzian−Gaussian window functions during postacquisition processing; otherwise, they contribute to peak broadening and require spin simulation to be detectable.[11] Not only to support the structural assignments but also to provide reference points for the structure elucidation of the new higher oligomers, **5** and **6**, complete ^{1}H NMR assignments of **3** and **4** were performed by ^{1}H iterative full spin analysis (HiFSA) using the PERCH software tool.[23,24] Quantum-mechanical total line shape (QMTLS) iteration of the spectra was repeated until the total root-mean-square (RMS) values were <0.1, representing excellent agreement between the simulated and observed spectra. By this means, the ^{1}H spin parameters (δ_H and $^{n}J_{H,H}$) of **3** and **4** were determined with high precision (δ_H, 0.1 ppb; *J*, 10 mHz; Table 2).

As we had developed the HiFSA profiles of **1** and **2** recently,[11] the availability of HiFSA data for **3** and **4** enabled a comparison of the ^{1}H NMR fingerprints of all four possible 4→8/2→*O*→7 doubly linked diastereomeric dimers (**1**−**4**). Their stacked ^{1}H and ^{13}C DEPTQ 135 NMR spectra are shown in Figure 4. From these unprecedented assignments of a coherent set of dimers, the ^{1}H and ^{13}C chemical shift differences ($\Delta\delta$) between the diastereomeric pairs **1**/**3** (2,3-trans = catechin/*ent*-catechin lower unit) and **2**/**4** (2,3-cis = epicatechin/*ent*-

DOI: 10.1021/acs.joc.6b02161
J. Org. Chem. 2017, 82, 1316−1329

Table 3. ^{1}H (900 MHz) and ^{13}C (225 MHz) NMR Spectroscopic Data of Compounds 5 and 6[a,b]

		5		6				5		6	
unit/ring	no.	δ_C, mult	δ_H (J, Hz)	δ_C, mult	δ_H (J, Hz)	unit/ring	no.	δ_C, mult	δ_H (J, Hz)	δ_C, mult	δ_H (J, Hz)
			unit I						unit III		
C	2	99.98, C		100.00, C		I	2	84.53, CH	4.6620, ddd (8.2, 0.1,-0.5)	100.38, C	
	3	68.59, CH	4.0246, d (3.1)	68.48, CH	3.9870, d (3.0)		3	68.46, CH	4.0860, ddd (8.7, 8.2, 5.7)	67.73, CH	4.0867, d (3.4)
	4	29.82, CH	4.6816, d (3.1)	29.78, CH	4.6718, d (3.0)		4	29.58, CH_2	3.0091, dd (−16.5, 5.7)	29.63, CH	4.3001, d (3.4)
									2.5730, ddd (−16.5, 8.7,0.5)		
A	5	157.84, C		157.90, C		G	5	156.13, C		150.70, C	
	6	97.74, CH	6.0059, d (2.4)	97.74, CH	6.0327, d (2.3)		6	96.28, CH	6.0862, s	110.18, C	
	7	158.11, C		158.15, C			7	152.70, C		152.96, C	
	8	96.33, CH	6.0483, d (2.4)	96.34, CH	6.0610, d (2.3)		8	107.33, C		97.27, CH	6.2523, s
	9	154.33, C		154.35, C			9	151.12, C		152.73, C	
	10	103.67, C		103.55, C			10	103.28, C		106.36, C	
B	1′	132.67, C		132.62, C		H	1′	130.79, C		132.09, C	
	2′	115.42, CH	7.0972, dd (2.2, 0.2)	115.21, CH	7.0325, dd (2.2, 0.2)		2′	116.03, CH	6.9638, ddd (2.1, −0.5, <0.1[c])	*115.59, CH	7.1191, dd (2.2, < 0.1[c])
	3′	145.61, C		145.56, C			3′	146.76, C		145.72, C	
	4′	146.27, C		146.65, C			4′	146.70, C		146.92, C	
	5′	115.64, CH	6.7815, dd (8.3, 0.2)	*115.61, CH	6.7469, dd (8.4, 0.2)		5′	116.26, CH	6.8303, dd (8.2, < 0.1[c])	*115.60, CH	6.8077, dd (8.3, <0.1[c])
	6′	119.65, CH	6.9929, dd (8.3, 2.2)	119.76, CH	6.9858, dd (8.4, 2.2)		6′	120.73, CH	6.8829, dd (8.2, 2.1)	119.83, CH	7.0109, dd (8.3, 2.2)
			unit II						unit IV		
F	2	100.76, C		100.95, C		L	2			85.00, CH	4.6119, ddd (9.1, −0.2, 0.1)
	3	67.82, CH	4.0997, d (3.2)	67.57, CH	4.1187, d (3.1)		3			68.01, CH	4.2543, ddd (9.1,9.1,6.1)
	4	29.65, CH	4.3194, d (3.2)	30.15, CH	4.3878, d (3.1)		4			30.61, CH_2	3.1288 dd (−16.4, 6.1)
											2.5768, ddd (−16.4, 9.1,0.1)
D	5	155.85, C		155.51, C		J	5			156.31, C	
	6	98.12, CH	6.1168, s	98.11, CH	6.1955, s		6			96.61, CH	6.0824, s
	7	153.45, C		153.56, C			7			152.26, C	
	8	108.80, C		109.12, C			8			106.38, C	
	9	148.97, C		148.89, C			9			151.69, C	
	10	105.42, C		105.19, C			10			103.71, C	
E	1′	132.41, C		132.31, C		K	1′			130.22, C	
	2′	115.50, CH	7.4033, dd (2.2, 0.2)	115.53, CH	7.4221, dd (2.2, < 0.1[c])		2′			117.27, CH	7.0656, ddd (2.0, −0.2, 0.2)
	3′	145.61, C		145.62, C			3′			146.23, C	
	4′	146.89, C		146.86, C			4′			147.06, C	
	5′	115.68, CH	6.8809, dd (8.3, 0.2)	115.70, CH	6.8914, dd (8.3, < 0.1[c])		5′			116.69, CH	6.9201, dd (8.2, 0.2)
	6′	120.30, CH	7.4232, dd (8.3, 2.2)	120.34, CH	7.4374, dd (8.3, 2.2)		6′			121.04, CH	7.0707, dd (8.2, 2.0)

[a] ^{1}H and ^{13}C NMR data were acquired in methanol-d_6 at 298 K at 900 and 225 MHz, respectively. [b] The δ_H and J values including their signs were generated via ^{1}H iterative full spin analysis (HiFSA).[11] [c] Very small couplings were detected by HiFSA (for pms profiles, see the Supporting Information) and are essential for the line overall fit. Asterisks indicate that the signals are interchangeable.

DOI: 10.1021/acs.joc.6b02161
J. Org. Chem. 2017, 82, 1316−1329

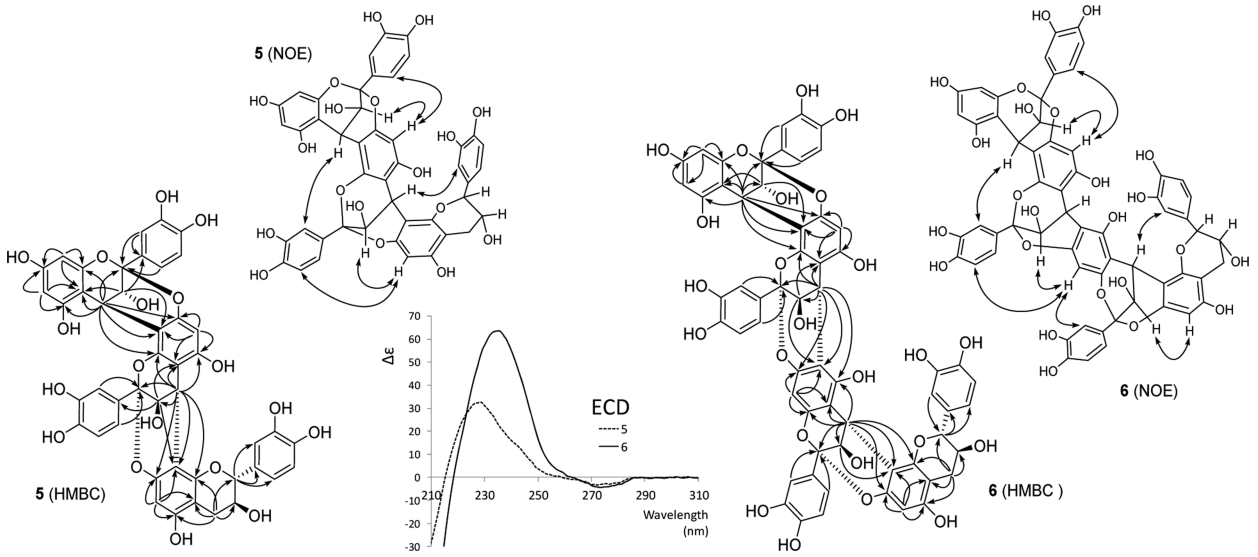

Figure 6. Key HMBC (H→C) and NOE (H↔H) correlations as well as ECD spectra of **5** and **6**.

epicatechin lower unit) could now be calculated and expressed in ppb, as shown in Figure 5. Only the chemical shift differences of C-3′ and C-4′ (B-rings) were excluded, as their assignments remained ambiguous. As expected, the pairwise chemical shift differences **1** vs **3** and **2** vs **4** were very small ($\Delta\delta_H$ < 0.13 ppm, $\Delta\delta_C$ < 1 ppm) but characteristic. Such subtle differences can be easily overlooked during dereplication or on identification of analogues. A detailed $\Delta\delta$ assessment in ppb revealed that the most diagnostic differences are I-H-3/6 (I designating the upper unit; note the difference to the customary designation of the I ring in **5** and **6**) and II-H-2/4b (lower unit) in ^{1}H NMR, as well as I- and II-C-2/9/10/2′/5′/6′ in the ^{13}C NMR profiles (Figure 5). This is in line with the prediction that the determination of the absolute configuration of individual flavan-3-ol monomeric units embedded in OPACs converts to the distinction of diastereomeric combinations of two or more units on analysis of OPACs with DP ≥ 2. This reduces the task at hand to the more manageable problem of relative configuration, provided unambiguous reference assignments are available, which in the present case involves **1**−**4**.

In the case of the ^{1}H NMR resonances in the E rings of the **1**/**3** diastereomeric pair, II-H-3 showed the greatest $\Delta\delta_H$ value of 92.5 ppb (Figure 5). The signals for I-H-3 also exhibited a relatively big difference with $\Delta\delta_H$ 53.2 ppb. On the other hand, the greatest $\Delta\delta_H$ of 124.6 ppb was observed for I-H-6 in the case of the **2**/**4** diastereomeric pair. The signals for I-H-3, II-H-2, and II-H-4b also showed noticeable differences with 101.7, 93.4, and 86.3 ppb, respectively.

In the ^{13}C NMR spectra, the resonances from the B rings of both of the upper and the lower units showed fairly large differences, which can be explained by diastereotopic effects arising from the molecular dynamics of the freely rotating B rings. While the magnitude of these effects predictably depends on conditions such as temperature, sample concentration, and pH, the present data indicate that the effects are negligible when same temperature is used, consistent sample concentrations are prepared (here 1−2 mg in 170 μL for 3 mm tubes), and the underivatized compounds are used in unbuffered organic solvent (here methanol-d_4). Therefore, the ^{13}C NMR resonances of the A and C ring core regions were identified as being diagnostic for the diastereomeric pairs, and the data presented provide reference for future work under similar conditions. Carbons II-C-2 and II-C-9 in the lower units (II) of both diastereomeric pairs, **1**/**3** and **2**/**4**, showed $\Delta\delta_c$ values of 577 ppb (II-C-2) vs 546 ppb (II-C-9), and 916 ppb (II-C-2) vs 843 ppb (II-C-9), respectively. These observations showed that select resonances are stereochemical indicators that allow the rapid, configurational dereplication of dimeric PACs with nearly identical NMR spectra.

Absolute Configurations of Unknown OPACs by Comparison of ^{13}C NMR Chemical Shifts. Provided that the *absolute* configuration at C-4 in the upper unit of an A-type dimer can be determined by ECD (here a positive Cotton effect in the region of 220−240 nm, indicating a 4*β* orientation), the configurations of the remaining stereogenic centers C-2 and C-3 in the lower unit can be gleaned from the ^{1}H NMR coupling patterns. Once this is established, determination of the absolute configurations at C-2 and C-3 in the lower unit of the A-type dimer boils down to a question of *relative* configurations. In other words, nonchiral NMR data should be able to determine the absolute configuration of the second unit, provided that the absolute configuration of the first unit is known. Accordingly, the diastereotopic ^{13}C NMR chemical shift patterns of the four possible 4→8/2→*O*→7 linked dimeric PACs (**1**−**4**) with fully known stereochemistry can serve as reference points for the *absolute* configuration at C-2 of the lower unit of other *unknown* doubly linked OPACs. In fact, the assignment only requires matching of congruent dimeric ^{13}C NMR shift patterns of **1**−**4** with those of the corresponding dimeric part of higher oligomerized PACs such as the new compounds **5** and **6**. The four diastereoisomers **1**−**4** are derived from epicatechin as the upper unit. As they resemble all possible base structures of the terminal units of **5** and **6**, they represent ideal starting points for the detailed structure elucidation of **5** and **6**.

Structure of the A-Type Trimer 5. The HR-ESI-MS based molecular formula of $C_{45}H_{34}O_{18}$ suggested **5** to be a trimer with two doubly linked A-type interflavanyl bonds. Its ^{1}H and ^{13}C DEPTQ-135 NMR spectra (Figures S17 and S18 in the Supporting Information) showed the resonances for three AMX spin systems, representing the presence of three 1,3,4-trisubstituted B, E, and H aromatic rings (compare with Table 3). The ^{1}H NMR spectrum of **5** also exhibited the resonances

DOI: 10.1021/acs.joc.6b02161
J. Org. Chem. 2017, 82, 1316−1329

for two AX systems at δ_H 4.0246 (d, J = 3.09 Hz, I-H-3) and 4.6816 (d, J = 3.09 Hz, I-H-4), as well as δ_H 4.0997 (d, J = 3.15 Hz, II-H-3) and 4.3194 (d, J = 3.15 Hz, II-H-4), indicating the presence of two doubly linked interflavanyl bonds. These connections were further supported by the presence of two acetal carbon resonances at δ_C 99.98 (I-C-2) and 100.76 (II-C-2). In addition, the appearance of the ^{1}H resonances at δ_H 4.6620 (ddd, J = 8.20, 0.54, −0.49 Hz, III-H-2), 4.0860 (ddd, J = 8.74, 8.20, 5.70 Hz, III-H-3), 3.0091 (dd, J = −16.45, 5.70 Hz, III-H-4a), and 2.5730 (ddd, J = −16.45, 8.74, 0.54 Hz, III-H-4b) suggested the 2,3-trans configured (*ent*-)catechin moiety to be the terminal unit of **5**. Doublet resonances for two meta-coupled protons at δ_H 6.0059 (J = 2.36 Hz, I-H-6) and 6.0483 (J = 2.36 Hz, I-H-8) as well as two one-proton singlets at δ_H 6.1168 (II-H-6) and 6.0862 (III-H-6) were assigned to the A ring protons of the flavan-3-ol constituent units. The presence of the 2→*O*→7/4→8 doubly linked interflavanyl bonds in **5** was confirmed by the HMBC cross-peaks from H-4 (C ring) to C-7 (δ 153.45), C-8 (δ 108.80), and C-9 (δ 148.97) of the D ring, and from H-4 (F ring) to C-7 (δ 152.70), C-8 (δ 107.33), and C-9 (δ 151.12) of the G ring (Figure 6). Furthermore, the 2→*O*→7/4→8 linkages were also confirmed by the observation of NOE correlations between H-4 (C ring) and H-2′ (E ring), as well as between H-4 (F ring) and H-2′ (H ring) (Figure 6). The 4*R* absolute configurations in the C and F rings were assigned on the basis of the 4β aryl orientation, as evidenced by the high-amplitude positive Cotton effects at 228 nm in the ECD spectrum (Figure 6).[21,22] Hence, the linkages between the units (I/II and II/III) were confirmed as (2β→O→7, 4β→8), which due to the C-2/C-4 relative configurations of A-type PACs must be cis.[25,26] Additionally, the 3,4-trans configurations of the C and F rings were deduced by the NOE cross-peaks between H-3 in the C ring and H-6 in the D ring, as well as between H-3 in the F ring and H-6 in the G ring, respectively.[27] Further analysis of 2D COSY, ROESY, HSQC, and HMBC correlation maps allowed the unambiguous assignments for all ^{1}H and ^{13}C NMR resonances of **5** (Figures S19−S22 in the Supporting Information).

It has been reported that flavan-3-ols with 2α and 2β configurations exhibited low-amplitude negative and positive ECD Cotton effects, respectively, in the 270−280 nm region.[28,29] However, the low-amplitude ECD signal derived from multiple C-2 positions of flavan-3-ols is hardly interpretable due to their signal accumulation.

The absolute configuration of the terminal flavan-3-ol unit was determined by comparison of the ^{13}C NMR chemical shifts of C-2 (δ_C 84.53) and C-9 (δ_C 151.12), which allowed differentiation of the two diastereoisomers **1** and **3**, with sufficient precision ($\Delta\delta_c \geq$ 0.50 ppm; Figure 7). Notably, the NMR spectra of **5** were similar to those of the known A-type trimer aesculitannin D (epicatechin-(2β→O→7,4β→8)-epicatechin-(2β→O→7,4β→8)-*ent*-catechin),[26,30] except for the ^{13}C NMR chemical shifts of C-2 (δ_C 83.9) and C-9 (δ_C 150.5).[27] This also supports the conclusion that the terminal unit of **5** is catechin rather than *ent*-catechin. This inference was further corroborated by gauge-independent atomic orbital (GIAO) ^{13}C NMR chemical shift calculations (Figures and Tables S34−S38 in the Supporting Information). Therefore, the structure of **5** was deduced as the new trimer epicatechin-(2β→O→7,4β→8)-epicatechin-(2β→O→7,4β→8)-catechin constitution.

Structure of the A-Type Tetramer 6. The starting point for the elucidation of **6** was the molecular formula of $C_{60}H_{44}O_{24}$ determined by HR-ESI-MS, which revealed that **6** is a

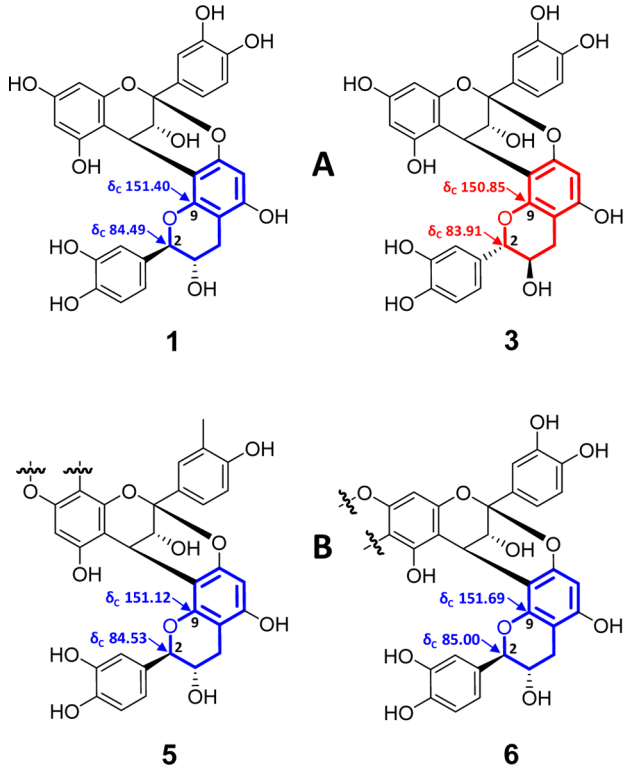

Figure 7. Carbon chemical shift comparison of the D and F ring cores of the model diastereoisomers **1** and **3** (A) with those of **5** and **6** (B), enabling the assignment of the absolute configurations at C-2 of the terminal units. The systematic evaluation of full $\Delta\delta_c$ maps of all four A-type dimers (Figure 5) led to the conclusion that the precise δ_c values of C-2 and C-9 are reliable indicators of the absolute configurations of terminal units in A-type OPACs.

tetrameric PAC with three A-type interflavanyl bonds. The ^{1}H and ^{13}C DEPTQ-135 NMR spectra (Figures S23 and S24 in the Supporting Information) of **6** showed high similarity with those of **5**, except for additional signals from one flavan-3-ol unit (Table 3). In the ^{1}H NMR spectrum, the doublets for two meta-coupled protons at δ_H 6.0327 (J = 2.33 Hz, I-H-6) and 6.0610 (J = 2.33 Hz, I-H-8) and three singlets at δ_H 6.1955 (II-H-6), 6.2523 (III-H-8), and 6.0824 (IV-H-6) were observed for the A rings of the flavan-3-ol moieties in **6**. The resonances for four AMX spin systems (B, E, H, and K rings) appeared in the aromatic region in the ^{1}H NMR spectra as well. In addition, the resonances for three AX spin systems (δ_H 3.9870 (d, J = 3.04 Hz, I-H-3) and 4.6718 (d, J = 3.04 Hz, I-H-4); 4.1187 (d, J = 3.05 Hz, II-H-3) and 4.3878 (d, J = 3.05 Hz, II-H-4); 4.0867 (d, J = 3.42 Hz, III-H-3) and 4.3001 (d, J = 3.42 Hz, III-H-4)) indicated the presence of three doubly linked flavan-3-ol moieties. This was further supported by the resonances of three acetal carbons at δ_C 100.00 (I-C-2), 100.95 (II-C-2), and 100.38 (III-C-2). The presence of an (*ent*-)catechin moiety (2,3-trans) as the terminal unit was evidenced by a large vicinal coupling constant ($^3J_{H\text{-}2,H\text{-}3}$ = 9.05 Hz, L ring). The 2→*O*→7/4→8 linkages between units I/II and III/IV were determined by the HMBC cross-peaks from H-4 of the C and I rings to C-7, C-8, and C-9 of the D and J rings, which were also supported by NOE associations between H-4 of the C and I rings and H-2′ of the E and K rings (Figure 6). On the other hand, the HMBC correlations from H-4 of the F ring to C-5 (δ 150.70), C-6 (δ 110.18), and C-7 (δ 152.96) of the G ring substantiated the 2→*O*→7/4→6 linkage between units II and III. The 2→

DOI: 10.1021/acs.joc.6b02161
J. Org. Chem. 2017, 82, 1316−1329

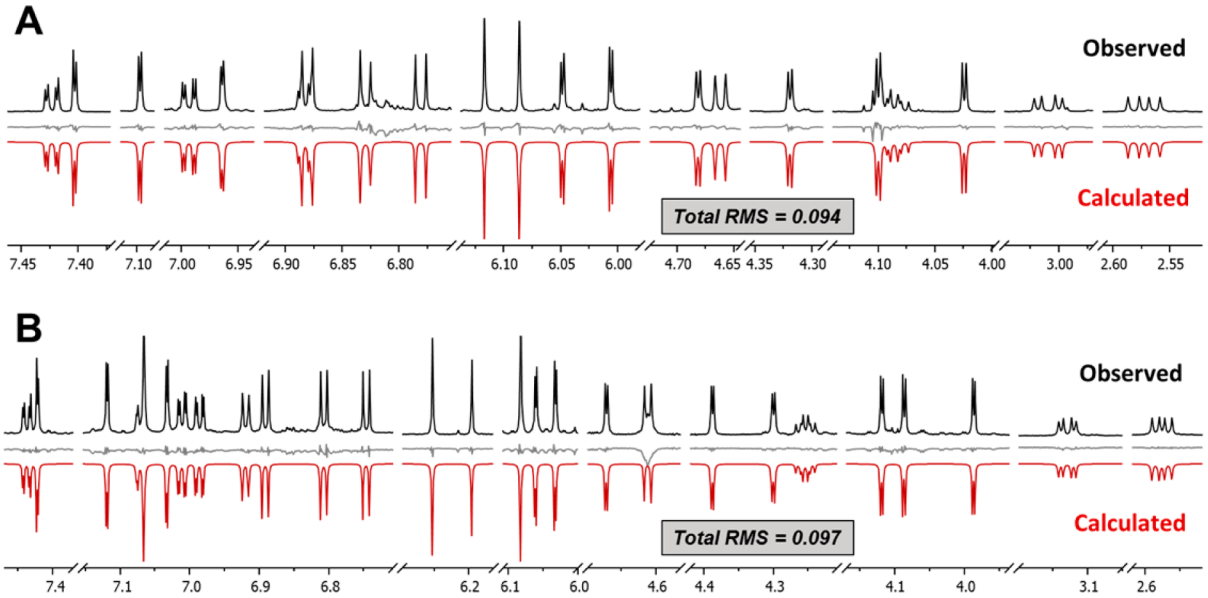

Figure 8. Comparison of the observed (black, obtained in methanol-d_6 at 900 MHz, 298 K) and calculated (red, generated by HiFSA) ^{1}H NMR spectra of **5** (A) and **6** (B), including residuals in gray.

O→7/4→6 linkage was proven by the presence of a downfield-shifted C-6 (III) carbon signal at δ_C 110.18: 4→6 linked structures show this typical C-6 chemical shift of δ_C 110−111 and, thus, can be distinguished from their 4→8 linked counterparts, which exhibit C-8 δ_C values of 106−108.[31] The NOE correlation between H-8 in the G ring and H-2′ of the H ring attested the presence of a 2→*O*→7/4→6 linkage (Figure 6). The 4β aryl orientations (C, F, and I rings) were also established by the strong positive ECD Cotton effects at 235 nm (Figure 6).[21,22] The NOE cross-peaks of H-3 (C ring)/H-6 (D ring), H-3 (F ring)/H-8 (G ring), and H-3 (I ring)/H-6 (J ring) revealed the 3,4-trans configurations of the C, F, and I rings.[27] All three NOE contacts were observed in a 900 MHz 2D NOESY experiment, while they were undetectable by 2D ROESY. This is in line with the general limitation of ROESY in capturing long-distance NOEs and explains the observation of relatively weak cross peaks for the analogous NOE contacts in the other molecules. The NOESY spectrum of **6** exhibited cross peaks in phase with the diagonal, indicating negative NOEs. Owing to the conformational rigidity of the A-type linkages, the possibility of chemical exchange leading to the observed in-phase cross peaks under spin diffusion conditions was ruled out.

Finally, in order to determine the absolute configurations at C-2 and C-3 in the terminal unit of **6**, the ^{13}C NMR chemical shifts of C-2 (δ_C 85.00) and C-9 (δ_C 151.69) were compared with those of the diastereomeric reference compounds, **1** and **3**, in the same way as described for **5** (Figure 7). This established that the terminal unit in **6** is also a catechin rather than an *ent*-catechin. Further support for this conclusion came from GIAO ^{13}C NMR chemical shift calculations (Figures and Tables S34−S38 in the Supporting Information). Collectively, the ^{13}C and comprehensive 2D NMR experiments (COSY, ROESY, NOESY, HSQC, HMBC; Figures S25−S29 in the Supporting Information) allowed unambiguous assignments for all ^{1}H and ^{13}C NMR resonances of **6** (Table 3). Accordingly, the structure of **6** was most compatible with that of the new tetramer epicatechin-(2β→O→7,4β→8)-epicatechin-(2β→O→7,4β→6)-epicatechin-(2β→O→7,4β→8)-catechin. This marks the first description of a tetramer exclusively possessing A-type interflavanyl linkages.

Full Spin Analysis of Compounds 5 and 6. In order to complete the interpretation and support future dereplication as well as ^{1}H NMR based elucidation of OPACs with DP ≥ 3, a complete ^{1}H NMR assignment was performed for **5** and **6** by means of ^{1}H iterative full spin analysis (HiFSA), using the same approach as described for **3** and **4**.[23,24] The achieved RMS values of the final simulated spectra were 0.094 for **5** and 0.097 for **6**, which represents excellent agreement with the observed spectra (Figure 8; residuals in gray). Thus, the true ^{1}H spin parameters (δ_H and $^nJ_{H,H}$) of **5** and **6** could be determined with high precision (δ_H, 0.1 ppb; *J*, 10 mHz) (Table 3). It should be pointed out that **6** is the highest molecular mass OPAC for which ^{1}H full spin analysis has been performed to date and at 1148 amu represents the second largest molecule overall, after the 1599 amu tridecapeptide ecumicin,[32] for which such an analysis has been performed.

■ CONCLUSIONS

Although OPACs have a wide range of biological effects and medicinal uses, their intrinsic, highly complex structural characteristics continue to make the pinpointing of individual structures and subsequent chemical standardization of health products challenging. OPACs are composed of a deceptively small number of near-identical monomers, which occur naturally in different absolute configurations, generating an incredible number of different oligomers with distinct three-dimensional molecular shapes. The determination of the absolute configuration of the monomeric moieties within an individual oligomer of DP ≥ 3 remains a difficult task. All methods available to date require chemical degradation, which is laborious, typically precludes biological evaluation due to sample loss, and by default is incapable of assessing the chemical properties of the entire molecule. Considering that the 3D molecular shape of OPACs is crucial for their specific biological activity, which depends on their interactions with biomolecules in 3D space such as the collagen backbone of dentin investigated here, nondegradative spectroscopic meth-

DOI: 10.1021/acs.joc.6b02161
J. Org. Chem. 2017, 82, 1316−1329

ods are in demand to elucidate DP ≥ 3 OPAC structures, including their absolute configurations.

The present study fills this gap by showing that the absolute configuration of trimeric and tetrameric OPACs can be deduced by means of nonchiral NMR. Two underlying concepts enable this analysis: (i) the availability of a comprehensive sets of NMR reference data of the relevant dimeric OPACs, covering the stereochemical possibilities and backed by ECD/ORD data to secure their absolute stereochemical assignments, and (ii) the fact that elongation of these reference dimers with additional enantiomeric monomers in each step forms diastereomeric, not enantiomeric, trimers, tetramers, and higher OPACs and, therefore, is amenable to nonchiral spectroscopic analysis on the basis of reference data (aspect i). The elucidation of the constitutions of compounds **5** and **6** shows that particularly the intramolecular ^{13}C NMR chemical shift effects (scs) are sufficiently pronounced to allow absolute configurational assignment of the individual monomers and distinguish all potential diastereomeric possibilities. Aspect ii of this approach is conceptually similar to the widely used Mosher ester NMR method and is similar to other chiral determination methods that operate on the principle of derivatization with enantiopure reagents to form diastereomers that are distinguishable by empirical and/or computational methods.

Knowledge of the absolute configuration enhances the specificity with which the binding affinity of ligands (OPACs) to the nanobiomolecules (dentin structures) can be assessed. The conformational space of each individual OPAC adds an additional layer of complexity to the overall consideration. While, for example, molecular dynamics involving rotations around B-type interflavanyl bonds, leading to atropisomeric species, must be considered for the interactions with the large biomacromolecules, experimentally feasible approaches to assess these phenomena are currently lacking. However, it is obvious that the absolute configuration of the individual monomeric building blocks has a major effect on the overall shape of the oligomers and their biological activity. Thus, the stereochemical information gained in this study is crucial structural information about dentin bioactive OPACs and can shape the further design of clinical candidate materials with optimized dentin biomimetic effects. The long-term dentin enhancement stability study also supports the conclusion that optimum molecular sizes and shapes exist for dentin−ligand stabilization. The investigated trimers and tetramers showed a 2-fold effect by significantly increasing dentin stiffness and lowering enzymatic biodegradation of dentin molecules. Collectively, this adds evidence for trimeric and tetrameric PACs from pine barks being good candidates for clinical intervention materials that can increase the longevity of dental restorations.

Regarding the broader goal of discovering new dentin-enhancing OPACs, a significant outcome of this study is the ability to assign the absolute configuration of more highly oligomerized molecules (DP ≥ 3) via subtle differences in the NMR chemical shifts and, thereby, determine vital structural information for dentin biomodifiers. The presented NMR approach is the first nondestructive method for this purpose and works with mass-limited samples. While the isolation yields for **5** and **6** were insufficient for the same bioassays used to assess the crude extracts and fractions, they are available for future less demanding mechanistic biological evaluations.

EXPERIMENTAL SECTION

General Methods. Optical rotation and ECD spectra were measured on a polarimeter and a circular dichroism spectrometer, respectively, at 25 °C in methanol. Mass spectrometry was carried out with an IT-TOF hybrid mass spectrometer. The 1D and 2D NMR measurements were performed on 600 and 900 MHz spectrometers equipped with TXI and TCI cryoprobes, respectively, using methanol-d_4 as the solvent. All NMR experiments were recorded at 298 K. The chemical shifts of the residual solvent signals at δ_H 3.3100 and δ_C 49.00 were used as the chemical shift references. Chemical shifts are given with 0.1 ppb decimal precision (not accuracy) for ^1H and 1 ppb for ^{13}C, in order to be adequate for the HiFSA results and the description of scs effects related to the absolute configuration of individual catechin monomers. The ^1H NMR data were processed using a Lorentzian−Gaussian window function (line broadening −0.3, Gaussian factor 0.05) prior to Fourier transformation. Silica gel (230−400 mesh) and Sephadex LH-20 were used for column chromatography. An HPTLC automatic sampler was used to increase reproducibility, precision, and dispersion of the HPTLC experiments. HPTLC was performed on Nano-SIL-20/UV_{254} (0.20 mm layer thickness, glass sheet) plates with visualization under UV light (254 and 365 nm) and vanillin−sulfuric acid reagent spray followed by heating (120 °C, 5 min). Normal phase profiles of VLC fractions were obtained by a HPLC instrument equipped with a photodiode array detector using a Develosil Diol (250 × 4.6 mm, 5 μm) column. Preparative HPLC was carried out using the same HPLC system, using the YMC-Pack ODS-AQ (250 × 10 mm, S-5, 12 nm) column.

Plant Material. Extract powder of the inner bark of *Pinus massoniana* was purchased from Xi'an Chukang Biotechnology in China in 2012 (No. PB120212).

Preparation of Pine OPAC Fractions by VLC. The extract (10 g) was subjected to silica gel vacuum liquid chromatography (VLC, 10 × 20 cm packing) using CH_2Cl_2 (A) and 1% water in MeOH (B) as a gradient solvent system (A/B = 95/5 to 50/50), affording 35 fractions (F01−F35).

HPTLC Profiling. Each pine VLC fraction was dissolved in MeOH at 1 mg/mL. An HPTLC instrument was used to spot the solutions on the HPTLC plate, which was developed with CH_2Cl_2/MeOH/water/formic acid (70/30/2/2). Figure 1 shows that each extract contains PACs with sufficient R_f distribution.

Diol HPLC Profiling. Each pine VLC fraction was prepared in methanol at a concentration of 10 mg/mL. Each fraction was eluted with a gradient solvent system ((A) acetonitrile/acetic acid 98/2, (B) MeOH/water/acetic acid 95/3/2) according to a method reported in the literature.[33] The chromatograms were monitored by a PDA detector at 280 nm.

Dentin Biomechanical Assay (0, 6, and 12 Months). Human molars were prepared for dentin biomechanical assay after approval by the Institutional Review Board Committee of University of Illinois at Chicago (protocol No. 2011-0312). Teeth were cut into 0.5 × 1.7 × 6.0 (H × W × L) mm dentin beams, demineralized using phosphoric acid, and treated with VLC fractions prepared at 0.65% w/v concentration at pH 7.2 (n = 10). The apparent modulus of elasticity (expressed in MPa) was performed on a universal testing machine using untreated dentin beams as controls as previously described.[12,34] The beams were tested immediately and after 6 and 12 months storage in simulated body fluid.[35]

Isolation of OPACs 3−6. As VLC fractions enriched with trimeric to tetrameric PACs showed higher dentin biomodification activities, a subsequent scale-up purification was performed by open column chromatography to identify bioactive individual molecules. The extract (100 g) was fractionated by silica gel open column chromatography (10 × 80 cm packing) using a gradient solvent system of dichloromethane and 1% water in methanol (98/2 to 50/50) to give 42 fractions (F01−F42). Subfraction F16 (4.0 g) was further separated by silica gel column chromatography (3 × 40 cm) using a $CHCl_3$/MeOH/water gradient (90/10/1 to 70/30/1) to afford 20 subfractions (F16.01−F16.20). Compounds **3** (1.2 mg) and **4** (1.5 mg) were isolated from subfraction F16.08 (200 mg) by HPLC using a

DOI: 10.1021/acs.joc.6b02161
J. Org. Chem. 2017, 82, 1316−1329

semipreparative C_{18} reverse-phase column with an isocratic solvent system of acetonitrile/0.1% formic acid in water (20/80). Subfraction F16.13 (50 mg) was also further separated by semipreparative HPLC using a C_{18} reverse-phase column with an isocratic solvent system of acetonitrile/0.1% formic acid in water (20/80), to give **5** (1.4 mg). Subfraction F19 (2 g) was chromatographed over Sephadex LH-20 (4 × 33 cm) with MeOH/water (70/30) followed by acetone/water (50/50) and finally by acetone/water (70/30) to afford 15 subfractions (F19.01−F19.15). Further purification of subfraction F19.13 (80 mg) was performed by semipreparative HPLC with a C_{18} reverse-phase column using an isocratic solvent system of acetonitrile/0.1% formic acid in water (22/78), to yield **6** (1.2 mg).

*Epicatechin-(2β→O→7,4β→8)-ent-catechin (procyanidin A4, **3**):* white powder; ECD (MeOH) λ_{max} ($\Delta\varepsilon$) 223 (+22.89), 271 (−2.97) nm; ^{1}H and ^{13}C NMR, see Table 2.

*Epicatechin-(2β→O→7,4β→8)-ent-epicatechin (**4**):* white powder; ECD (MeOH) λ_{max} ($\Delta\varepsilon$) 223 (+36.38), 271 (−3.56) nm; ^{1}H and ^{13}C NMR, see Table 2.

*Epicatechin-(2β→O→7,4β→8)-epicatechin(2β→O→7,4β→8)-catechin (**5**):* brown, amorphous solid; $[\alpha]^{25}_{D}$ = +22.22 (*c* 0.12, MeOH); ECD (MeOH) λ_{max} ($\Delta\varepsilon$) 228 (+32.64), 272 (−3.28) nm; ^{1}H and ^{13}C NMR, see Table 3; HRESIMS $[M - H]^-$ *m*/*z* 861.1641 (calcd for $C_{45}H_{33}O_{18}$, 861.1667).

*Epicatechin-(2β→O→7,4β→8)-epicatechin-(2β→O→7,4β→6)-epicatechin-(2β→O→7,4β→8)-catechin (**6**):* brown, amorphous solid; $[\alpha]^{25}_{D}$ = +39.18 (*c* 0.10, MeOH); ECD (MeOH) λ_{max} ($\Delta\varepsilon$) 235 (+63.68), 273 (−4.40) nm; ^{1}H and ^{13}C NMR, see Table 3; HRESIMS $[M + H]^+$ *m*/*z* 1149.2287 (calcd for $C_{60}H_{45}O_{24}$, 1149.2295).

Computational Analysis. The ^{1}H iterative full spin analysis (HiFSA) was performed using the PERCH NMR software package (version 2013.1, PERCH Solutions Ltd., Kuopio, Finland) as reported previously.[24,36] The final optimized ^{1}H NMR spectral parameters of **3**−**6** are attached as tabulated HiFSA profiles in the PERCH .pms file format (Tables S30−S33 in the Supporting Information). Chemical shifts (δ_H in ppm) and coupling constants (*J* in Hz) are reported with four and two decimal place precision, respectively. Quantum-chemical calculations of the ^{13}C NMR chemical shifts for the epimer pairs of **5a**/**5b** and **6a**/**6b** were carried out for the determination of the absolute configurations. The 3D geometries of these compounds were first optimized in the MM2 force field by ChemOffice software then in the B3LYP/6-31G(d) level by quantum-chemical DFT calculations in Gaussian 09 software.[37] The B3LYP/6-31G(d) harmonic vibrational frequencies were further calculated to confirm their stability. Gauge-independent atomic orbital (GIAO) calculations of ^{13}C NMR chemical shifts were accomplished by density functional theory (DFT) at the rmpw1pw91/6-31+g(d,p) level. The ^{13}C NMR chemical shifts for TMS were calculated by the same procedure and used as the reference.[37] DP4 analysis was employed to determine the best fit to the experimental data (^{13}C NMR chemical shifts) from the diastereomeric models via applets from http://www-jmg.ch.cam.ac.uk/tools/nmr/DP4/.

Binary analytical data (original (q)NMR FIDs, spreadsheets, PMS files) are available upon request and DOI http://dx.doi.org/10.7910/DVN/NEWLHE.

■ ASSOCIATED CONTENT

Supporting Information

The Supporting Information is available free of charge on the ACS Publications website at DOI: 10.1021/acs.joc.6b02161.

1D/2D NMR spectra, qHNMR profiles, tabulated ^{1}H NMR profiles (transcript of HiFSA result in PERCH.pms file) of **3**−**6**, the optimized lowest energy 3D conformers of **5** (**5a**/**5b**) and **6** (**6a**/**6b**), gauge-independent atomic orbital (GIAO) calculations of ^{13}C NMR chemical shifts, and absolute energies and atom coordinates of conformers of **5** (**5a**/**5b**) and **6** (**6a**/**6b**) (PDF)

■ AUTHOR INFORMATION

Corresponding Author

*E-mail for G.F.P.: gfp@uic.edu.

ORCID

Shao-Nong Chen: 0000-0003-0748-0863

Guido F. Pauli: 0000-0003-1022-4326

Notes

The authors declare no competing financial interest.

■ ACKNOWLEDGMENTS

The research at the University of Illinois at Chicago was supported by grant R01 DE021040 from NIDCR/NIH. The construction of the UIC CSB and the purchase of the 900 MHz NMR spectrometer was generously funded by a grant to Dr. Peter Gettins from NIGMS Grant No. P41 GM068944. Dr. B. Ramirez is acknowledged for his valued support in the NMR facility at the UIC Center for Structural Biology (CSB). The authors are grateful to one reviewer for helpful comments regarding the absolute configuration of oligomeric proanthocyanidins.

■ REFERENCES

(1) Selwitz, R. H.; Ismail, A. I.; Pitts, N. B. *Lancet* **2007**, *369*, 51−59.
(2) Shenoy, A. *J. Conservative Dent.* **2008**, *11*, 99−107.
(3) *Future Use of Materials for Dental Restoration*; World Health Organization, 2009.
(4) Demarco, F. F.; Collares, K.; Coelho-de-Souza, F. H.; Correa, M. B.; Cenci, M. S.; Moraes, R. R.; Opdam, N. J. *Dent. Mater.* **2015**, *31*, 1214−1224.
(5) Bedran-Russo, A. K.; Pauli, G. F.; Chen, S.-N.; McAlpine, J. B.; Castellan, C. S.; Phansalkar, R. S.; Aguiar, T. R.; Vidal, C. M. P.; Napolitano, J. G.; Nam, J.-W.; Leme, A. A. *Dent. Mater.* **2014**, *30*, 62−76.
(6) Bedran-Russo, A. K.; Pashley, D. H.; Agee, K.; Drummond, J. L.; Miescke, K. J. *J. Biomed. Mater. Res., Part B* **2008**, *86B*, 330−334.
(7) He, L.; Mu, C.; Shi, J.; Zhang, Q.; Shi, B.; Lin, W. *Int. J. Biol. Macromol.* **2011**, *48*, 354−359.
(8) Vidal, C. M. P.; Leme, A. A.; Aguiar, T. R.; Phansalkar, R. S.; Nam, J.-W.; Bisson, J.; McAlpine, J. B.; Chen, S.-N.; Pauli, G. F.; Bedran-Russo, A. K. *Langmuir* **2014**, *30*, 14887−14893.
(9) Leme-Kraus, A. A.; Aydin, B.; Vidal, C. M. P.; Phansalkar, R. S.; Nam, J.-W.; McAlpine, J. B.; Pauli, G. F.; Chen, S.-N.; Bedran-Russo, A. K. *J. Dent. Res.* **2016**, 0022034516680586.
(10) Phansalkar, R. S.; Nam, J.-W.; Chen, S.-N.; McAlpine, J. B.; Napolitano, J. G.; Leme, A. A.; Vidal, C. M. P.; Aguiar, T.; Bedran Russo, A. K.; Pauli, G. F. *Fitoterapia* **2015**, *101*, 169−178.
(11) Nam, J.-W.; Phansalkar, R. S.; Lankin, D. C.; Bisson, J.; McAlpine, J. B.; Leme, A. A.; Vidal, C. M. P.; Ramirez, B.; Niemitz, M.; Bedran-Russo, A. K.; Chen, S.-N.; Pauli, G. F. *J. Org. Chem.* **2015**, *80*, 7495−7507.
(12) Aguiar, T. R.; Vidal, C. M. P.; Phansalkar, R. S.; Todorova, I.; Napolitano, J. G.; McAlpine, J. B.; Chen, S.-N.; Pauli, G. F.; Bedran-Russo, A. K. *J. Dent. Res.* **2014**, *93*, 417−422.
(13) Ferreira, D.; Slade, D. *Nat. Prod. Rep.* **2002**, *19*, 517−541.
(14) Ferreira, D.; Li, X.-C. *Nat. Prod. Rep.* **2000**, *17*, 193−212.
(15) Steynberg, P. J.; Cronje, A.; Steynberg, J. P.; Bezuidenhoudt, B. C. B.; Brandt, E. V.; Ferreira, D. *Tetrahedron* **1997**, *53*, 2591−2598.
(16) Kennedy, J. A.; Jones, G. P. *J. Agric. Food Chem.* **2001**, *49*, 1740−1746.
(17) Lou, H.; Yamazaki, Y.; Sasaki, T.; Uchida, M.; Tanaka, H.; Oka, S. *Phytochemistry* **1999**, *51*, 297−308.
(18) Lu, W.-C.; Huang, W.-T.; Kumaran, A.; Ho, C.-T.; Hwang, L. S. *J. Agric. Food Chem.* **2011**, *59*, 6214−6220.
(19) Zhang, H.; Yerigui; Yang, Y.; Ma, C. *J. Agric. Food Chem.* **2013**, *61*, 8814−8820.

DOI: 10.1021/acs.joc.6b02161
J. Org. Chem. 2017, 82, 1316−1329

(20) Pauli, G. F.; Chen, S.-N.; Simmler, C.; Lankin, D. C.; Gödecke, T.; Jaki, B. U.; Friesen, J. B.; McAlpine, J. B.; Napolitano, J. G. *J. Med. Chem.* **2014**, *57*, 9220−9231.
(21) Botha, J. J.; Young, D. A.; Ferreira, D.; Roux, D. G. *J. Chem. Soc., Perkin Trans. 1* **1981**, 1213−1219.
(22) Ding, Y.; Li, X.; Ferreira, D. *J. Nat. Prod.* **2010**, *73*, 435−440.
(23) Napolitano, J. G.; Lankin, D. C.; Graf, T. N.; Friesen, J. B.; Chen, S.-N.; McAlpine, J. B.; Oberlies, N. H.; Pauli, G. F. *J. Org. Chem.* **2013**, *78*, 2827−2839.
(24) Napolitano, J. G.; Lankin, D. C.; Chen, S.-N.; Pauli, G. F. *Magn. Reson. Chem.* **2012**, *50*, 569−575.
(25) Bilia, A. R.; Morelli, I.; Hamburger, M.; Hostettmann, K. *Phytochemistry* **1996**, *43*, 887−892.
(26) Chen, L.; Yuan, P.; Chen, K.; Jia, Q.; Li, Y. *Food Chem.* **2014**, *154*, 315−322.
(27) Cronje, A.; Burger, J. F. W.; Brandt, E. V.; Kolodziej, H.; Ferreira, D. *Tetrahedron Lett.* **1990**, *31*, 3789−3792.
(28) Slade, D.; Ferreira, D.; Marais, J. P. J. *Phytochemistry* **2005**, *66*, 2177−2215.
(29) Van Rensburg, H.; Steynberg, P. J.; Burger, J. F. W.; Van Heerden, P. S.; Ferreira, D. *J. Chem. Res., Synop.* **1999**, 450−451.
(30) Morimoto, S.; Nonaka, G.; Nishioka, I. *Chem. Pharm. Bull.* **1987**, *35*, 4717−4729.
(31) Tamura, T.; Inoue, N.; Ozawa, M.; Shimizu-Ibuka, A.; Arai, S.; Abe, N.; Koshino, H.; Mura, K. *Biosci., Biotechnol., Biochem.* **2013**, *77*, 1306−1309.
(32) Gao, W.; Napolitano, J. G.; Lankin, D. C.; Kim, J.-Y.; Jin, Y.-Y.; Lee, H.; Suh, J.-W.; Chen, S.-N.; Pauli, G. F. *Magn. Reson. Chem.* **2016**, DOI: 10.1002/mrc.4425.
(33) Robbins, R. J.; Leonczak, J.; Johnson, J. C.; Li, J.; Kwik-Uribe, C.; Prior, R. L.; Gu, L. *J. Chromatogr. A* **2009**, *1216*, 4831−4840.
(34) Vidal, C. M. P.; Aguiar, T. R.; Phansalkar, R. S.; McAlpine, J. B.; Napolitano, J. G.; Chen, S.-N.; Araujo, L. S. N.; Pauli, G. F.; Bedran-Russo, A. K. *Acta Biomater.* **2014**, *10*, 3288−3294.
(35) Leme, A. A.; Vidal, C. M. P.; Hassan, L. S.; Bedran-Russo, A. K. *J. Biomech.* **2015**, *48*, 2067−2071.
(36) Napolitano, J. G.; Lankin, D. C.; McAlpine, J. B.; Niemitz, M.; Korhonen, S.-P.; Chen, S.-N.; Pauli, G. F. *J. Org. Chem.* **2013**, *78*, 9963−9968.
(37) Frisch, M. J.; Trucks, G. W.; Schlegel, H. B.; Scuseria, G. E.; Robb, M. A.; Cheeseman, J. R.; Scalmani, G.; Barone, V.; Mennucci, B.; Petersson, G. A.; Nakatsuji, H.; Caricato, M.; Li, X.; Hratchian, H. P.; Izmaylov, A. F.; Bloino, J.; Zheng, G.; Sonnenberg, J. L.; Hada, M.; Ehara, M.; Toyota, K.; Fukuda, R.; Hasegawa, J.; Ishida, M.; Nakajima, T.; Honda, Y.; Kitao, O.; Nakai, H.; Vreven, T.; Montgomery, J. A., Jr.; Peralta, J. E.; Ogliaro, F.; Bearpark, M. J.; Heyd, J.; Brothers, E. N.; Kudin, K. N.; Staroverov, V. N.; Kobayashi, R.; Normand, J.; Raghavachari, K.; Rendell, A. P.; Burant, J. C.; Iyengar, S. S.; Tomasi, J.; Cossi, M.; Rega, N.; Millam, N. J.; Klene, M.; Knox, J. E.; Cross, J. B.; Bakken, V.; Adamo, C.; Jaramillo, J.; Gomperts, R.; Stratmann, R. E.; Yazyev, O.; Austin, A. J.; Cammi, R.; Pomelli, C.; Ochterski, J. W.; Martin, R. L.; Morokuma, K.; Zakrzewski, V. G.; Voth, G. A.; Salvador, P.; Dannenberg, J. J.; Dapprich, S.; Daniels, A. D.; Farkas, Ö.; Foresman, J. B.; Ortiz, J. V.; Cioslowski, J.; Fox, D. J. *Gaussian 09*; Gaussian, Inc., Wallingford, CT, USA, 2009.

DOI: 10.1021/acs.joc.6b02161
J. Org. Chem. 2017, 82, 1316−1329